On the quantification and visualization of transient periodic instabilities in pulsatile flows

Author’s Accepted Manuscript

www.elsevier.com/locate/jbiomech

On the Quantification and Visualization of Transient Periodic Instabilities in Pulsatile Flows

Muhammad Owais Khan, Christophe Chnafa, Diego Gallo, Filippo Molinari, Umberto Morbiducci, David A. Steinman, Kristian Valen-Sendstad

PII: S0021-9290(16)31330-6
DOI: http://dx.doi.org/10.1016/j.jbiomech.2016.12.037
Reference: BM8070

To appear in: *Journal of Biomechanics*
Accepted date: 21 December 2016

Cite this article as: Muhammad Owais Khan, Christophe Chnafa, Diego Gallc Filippo Molinari, Umberto Morbiducci, David A. Steinman and Kristian Valen-Sendstad, On the Quantification and Visualization of Transient Periodic Instabilities in Pulsatile Flows, *Journal of Biomechanics* http://dx.doi.org/10.1016/j.jbiomech.2016.12.037

On the Quantification and Visualization of Transient Periodic Instabilities in Pulsatile Flows

Muhammad Owais Khan[a,d,*], Christophe Chnafa[a], Diego Gallo[b], Filippo Molinari[c], Umberto Morbiducci[b], David A. Steinman[a], Kristian Valen-Sendstad[d]

[a]Department of Mechanical and Industrial Engineering, University of Toronto, Toronto, ON, Canada
[b]Department of Mechanical and Aerospace Engineering, Politecnico di Torino, Torino, Italy
[c]Department of Electronics and Telecommunications, Politecnico di Torino, Torino, Italy
[d]Computational Cardiac Modeling Department, Simula Research Laboratory, Lysaker, Norway

Abstract

Turbulent-like flows without cycle-to-cycle variations are more frequently being reported in studies of cardiovascular flows. The associated stimuli might be of mechanobiological relevance, but how to quantify them objectively is not obvious. Classical Reynolds decomposition, where the flow is separated into mean and fluctuating velocity components, is not applicable as the phase-average is zero. We therefore expanded on established techniques and present the idea, analogous to Reynolds decomposition, to decompose a flow with transient instabilities into low- versus high frequency components, respectively, to discriminate flow instabilities from the underlying cardiac pulsatility. Transient wall shear stress and velocity signals derived from computational fluid dynamic simulations were transferred to the frequency domain. A high-pass filter was applied to subtract the 99% most-energy-containing frequencies, which gave a cut-off frequency of 25Hz. We introduce here the spectral power index, and compute the fluctuating kinetic energy, based on the high-pass filtered velocity components, both being frequency-based operators. The efficacy was evaluated in an aneurysm model for multiple flow rates demonstrating transition to turbulent-like flows. The frequency-based operators were found to better correlate with the qualitatively observed flow instabilities compared to conventional descriptors, like time-averaged wall shear stress or oscillatory shear index. We demonstrate how the high frequencies beyond the physiological range could be analyzed and/or transferred back to the time domain for quantification and visualization purposes. We have introduced general frequency-based operators, easily extendable to other cardiovascular territories based on a posteriori heuristic filtering that allows for separation, isolation, and quantification of cycle-invariant turbulent-like flows.

Keywords: Hemodynamics, Cycle-Invariant Turbulent-Like Flows, Visualization, Spectral Power Index, Fluctuating Kinetic Energy

1. Introduction

Hemodynamic forces, particularly wall shear stress (WSS), are thought to contribute to vessel wall adaption and remodeling (Malek et al., 1999; Morbiducci et al., 2016). Since direct measurements of these stresses are difficult, medical image-based computational fluid dynamics (CFD) (Taylor and Steinman, 2010)

*For correspondence: Kristian Valen-Sendstad, Simula Research Laboratory, Lysaker, Norway. Email: kvs@simula.no

has been extensively used in the investigation of vascular pathology. Except for aortic flows with Reynolds numbers (Re) in the thousands (Nerem et al., 1972), cardiovascular flows have conventionally been considered laminar and stable; however, recent advances in imaging tools, as well as focus on numerical accuracy have highlighted the presence of transitional and turbulent-like flows (Valen-Sendstad et al., 2011; Chnafa et al., 2014; Valen-Sendstad et al., 2014; Zajac et al., 2015), consistent with experimental evidence (Roach et al., 1972; Yagi et al., 2013) and clinical observations (Ferguson, 1970; Kurokawa et al., 1994). The arterial stimuli from such turbulent-like flows have been linked, both *in vivo* (Fry, 1968) and *in vitro* (Davies et al., 1986), to adverse vascular remodeling. However, there appears to be no consensus in the literature on how to robustly quantify such turbulent-like flows.

While methods for decomposing the mean and transient parts of truly turbulent flows are well understood (Pope, 2000), for pulsatile flows this can only be applied in a phase-averaged sense, for flows with instabilities that vary from cycle to cycle (Chnafa et al., 2014; Poelma et al., 2015). Proper orthogonal decomposition (Grinberg et al., 2009) is an alternative method that allows for distinction between flow phenotypes and higher fluctuating components in cycle-invariant flows. However, the mechanobiological relevance of hemodynamic stresses reconstructed from high-mode velocity fields requires further investigation. Instead, initial ad hoc attempts in the biomedical literature have been focused on analyzes or visualizations of 1D velocity-time traces from selected points (Valen-Sendstad et al., 2013; Bozzetto et al., 2015; Varble et al., 2016). However, these traces are subjectively placed, provide a limited amount of information, and do not allow for additional post-processing or make complete use of the available 3D flow field.

Conventional hemodynamic WSS-based descriptors like time-averaged WSS and Oscillatory Shear Index (OSI) were originally developed for unsteady laminar flow regimes, and thus are not necessarily adequate descriptors of turbulent-like flow stimuli. The aim of the current study was to investigate a robust approach to quantify and visualize these turbulent-like flows. We propose frequency-based operators, which, analogous to Reynolds decomposition, decompose a signal into low- and high-frequency components. We demonstrate how this method can be applied to detect, characterize, quantify, and visualize high-frequency instabilities of volumetric and surface quantities, focusing on a cerebral aneurysm as a representative example.

2. Methods

We took advantage of methods frequently used, e.g., in turbulence research (Pope, 2000), where any signal can be transferred from the time domain to the frequency domain. Taking this approach, any heuristic filter can be applied to analyze the low versus high frequency components, and (potentially) transfer the harmonics back to the time domain for additional analyses and visualization purposes. Analogous to Reynolds decomposition, the signal reconstructed from low- versus high-frequencies are comparable to the phase-average versus fluctuating components, respectively.

Figure 1 illustrates this principle where the 1D time-velocity trace in red was decomposed using a high pass filter. The low frequency physiological 'carrier' signal is shown in black, while the high frequency residual is shown in blue, reflecting the 'unphysiological' fluctuating components. We emphasize that this applies to any 1D signal, like velocity, pressure, or WSS trace, but can also be assembled to surface and volumetric quantities, respectively.

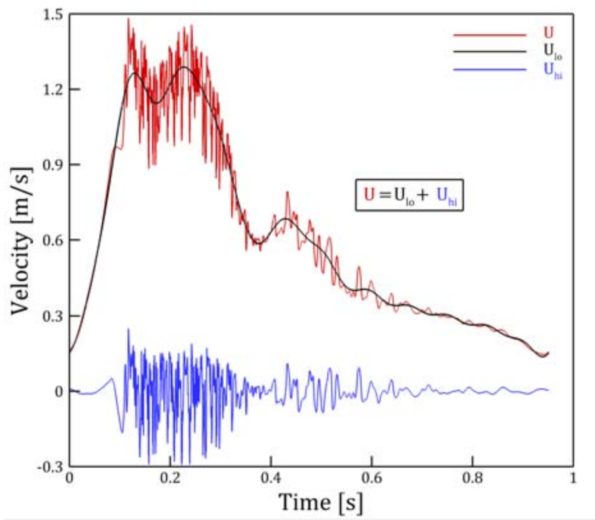

Figure 1: Visual representation of a cycle-invariant unstable flow and the of subtraction of the 99% most energy-containing-frequencies. The inset equation shows the analogy to Reynolds decomposition where U_{lo} is equivalent of the phase-average while U_{hi} is equivalent of the fluctuating component.

Inspired by the harmonic index defined as the fraction of harmonic amplitude spectrum arising from pulsatile flow component (Gelfand et al., 2006), we defined the spectral power index (SPI):

$$\mathrm{SPI} = \frac{\sum_{n=n_c}^{+\infty} |Y[n\omega_0]|^2}{\sum_{n=1}^{+\infty} |Y[n\omega_0]|^2} \tag{1}$$

Where $|Y[n\omega_0]|$ is the magnitude of the Fourier-transformed signal, ω_0 is the fundamental angular frequency of the periodic signal, n_c is the harmonic corresponding to the cut-off frequency. To objectively determine n_c in order to exclude frequencies in the normal physiological range, we subtracted harmonics that contained 99% of the energy in the driving flow rate waveform, which resulted in a cut-off frequency of n_c=25Hz. We emphasize two key differences from the harmonic index by Gelfand et al. (Gelfand et al., 2006): i) SPI does not include the pulsatile waveform mean in the denominator, such that summation begins from the first harmonic, ii) SPI is based on the power of the signal instead of the energy, to better highlight energy content at higher frequencies. SPI is, therefore, a normalised quantity having the desirable property of being on the interval $[0-1]$; zero meaning that there are no flow instabilities while the scalar value 1 would reflect a completely unstable flow. Analogous to turbulence kinetic energy (TKE), we also computed the time-averaged fluctuating kinetic energy (FKE), defined as:

$$\mathrm{FKE} = \frac{1}{2}(\overline{u_{hi}^2} + \overline{v_{hi}^2} + \overline{w_{hi}^2}) \tag{2}$$

In contrast to Varble et al. (2016) who used a steady inflow, we here applied eq. (2) to a pulsatile waveform where u_{hi}, v_{hi} and w_{hi} are the high-pass filtered velocity components and the overline refers to the time average. To evaluate the efficacy of frequency based operators, we chose an aneurysm model from the open-source Aneurisk database (Aneurisk-Team, 2012). We specified a fully developed Womersley velocity profile at the inlet, with a cross sectional mean velocity of .27 m/s (Valen-Sendstad et al., 2015) giving a base flow rate of Q = 5.37mL/s with a period of 0.951s. The flow rate was also reduced to .75Q, .5Q, and .25Q to demonstrate the onset of flow instabilities. The Vascular Modelling ToolKit (Antiga et al., 2008) was used to generate a mesh with four boundary layers that consisted of three million tetrahedron cells, equivalent in spatial resolution to the 'Medium' (HR5) simulations in (Khan et al., 2015), previously demonstrated to be sufficient to resolve WSS and OSI.

Pulsatile CFD simulations were performed using the CFD solver *Oasis*, taking 10,000 time steps per cycle. *Oasis* uses a projection scheme where special care has been taken to maintain a second-order accuracy in space and time (Simo and Armero, 1994) to obtain a solution that preserves kinetic energy while minimizes numerical dispersion and diffusion errors. For details regarding the implementation and order-optimal convergence results, we refer to (Mortensen and Valen-Sendstad, 2015). Post-processing was based on 2500 time steps, corresponding to Nyquist limit of 1314Hz. SPI applied to WSS-time traces (SPI_{WSS}) and FKE were then compared against nominal descriptors like the WSS normalised to the parent artery (TAWSS) and OSI.

3. Results

Figure 2 (a) shows the chosen model and velocity magnitude traces in the carotid siphon, middle cerebral artery and the aneurysmal sac for 0.25Q, 0.5Q, 0.75Q and Q. While traces for 0.25Q and 0.5Q do not feature evident high-frequency fluctuations, the complexity of the traces for 0.75Q and Q are indicative of a turbulent-like flow, especially in the aneurysm sac.

From the corresponding qualitative maps shown in Figure 2 (b), we note only a modest increase in the parent artery normalised TAWSS maps with increasing flow rates. Regions of elevated OSI were found for relatively stable flows 0.25Q and 0.5Q, but also for turbulent-like flows, 0.75Q and Q. This is reflected through the inset traces showing the WSS magnitudes recorded at a location on the sac dome marked with a circle. In short, locations of high OSI are relatively unaffected by flow rate; what is affected is their extent, but approximately linearly with flow rate. Broadly, these maps indicate that both TAWSS and OSI are unable to discriminate laminar from turbulent-like flow stimuli.

On the other hand, a distinct increase in SPI_{WSS} was observed between 0.5Q and 0.75Q, consistent with the appearance of higher-frequencies observed in filtered WSS time-magnitude traces, cf., inset figure. Evident from these plots is that SPI_{WSS} is sensitive to flow destabilization and is able to discriminate between stable and unstable stimuli. Similar trends were observed for cycle-averaged volumetric FKE maps;

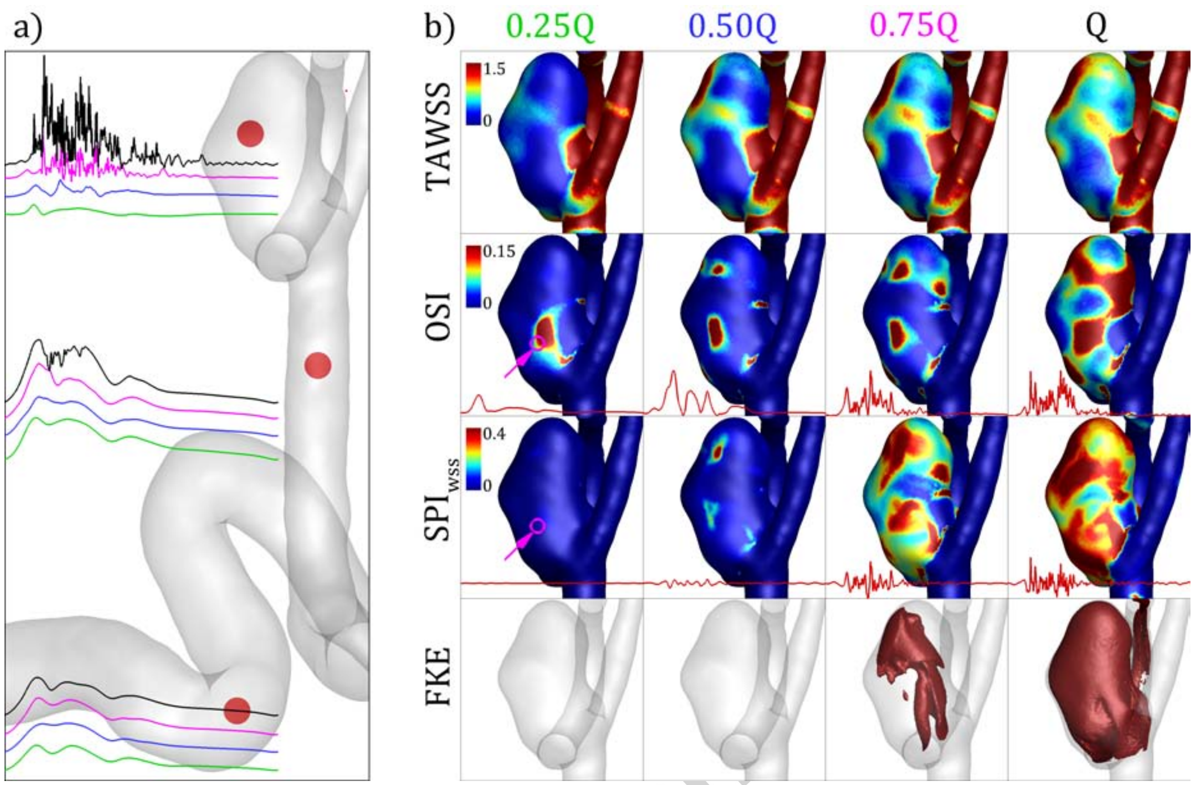

Figure 2: A) Chosen model and velocity traces at various locations normalised by the cycle mean. B) The hemodynamic indices TAWSS, OSI, SPI_{WSS}, and FKE for increasing flow rates.

no FKE is observed for 0.25Q and 0.5Q. However, distinct regions of FKE were observed for 0.75Q and Q, correlating with the presence of high-frequency instabilities in the flow.

Focusing now on quantitative results shown in Table 1, we note that while sac-averaged values of TAWSS and OSI increase approximately linearly as a function of flow rate, SPI_{WSS} and FKE show a sharp increase between 0.5Q and 0.75Q, correlating with the appearance of high-frequency flow fluctuations. Being primarily interested in the differences between 0.5Q and 0.75Q, we observe that SPI_{WSS} showed a 6-fold increase from 0.5Q to 0.75Q whereas TAWSS and OSI only increased by 20% and 70%, respectively.

Finally, as shown in the online supplementary material, animation of the high-pass filtered reconstructed velocity field better highlights the flow instabilities due to a narrower dynamic range, compared to an animation of the complete velocity field.

4. Discussion

Although all of the building blocks are well-known, we have described here general frequency-based operators for filtering, visualization, and analysis of turbulent-like flow features that can be assembled on surfaces and volumes. The concept is readily extendable to cycle-invariant turbulent-like flows of other cardiovascular territories, allowing for objective separation, isolation, and quantification of flow instabilities.

Table 1: Sac surface- or volume-averaged indices quantifying the marked increase for SPI_{WSS} and FKE, whereas TAWSS and OSI increase linearly with flow rates and/or time-averaged parent artery Reynolds number.

Flow rate	0.25Q	0.5Q	0.75Q	Q
Re [-]	97.5	195	292.5	390
TAWSS [-]	0.46	0.71	0.86	0.91
OSI [-]	0.013	0.024	0.041	0.096
SPI_{WSS} [-]	0.004	0.037	0.220	0.325
FKE $[m^2/s^2]$	0	0	0.003	0.011

In addition, this method can also be used for flows harbouring cycle-to-cycle fluctuations to separate inter-cycle and intra-cycle variations.

OSI is frequently argued to be a metric of 'disturbed flow', and has been demonstrated to be effective (Ku et al., 1985) even if incomplete descriptor (Gallo et al., 2016). However, it cannot discriminate slow, unidirectional oscillatory flow from fast, multidirectional variations, as shown in Figure 2 and discussed in previous studies (Peiffer et al., 2013; Valen-Sendstad and Steinman, 2014; Khan et al., 2015). As mentioned in the introduction, turbulent-like flows have been linked both *in vitro* and *in vivo* to adverse vascular remodeling. As an example, we previously reported an "intriguing albeit incidental" correlation between TKE and aneurysm rupture status (Valen-Sendstad et al., 2013), under steady state inflow. SPI is an example of a metric that is reduced to a single number allowing for mapping of hotspots of turbulent WSS under more realistic pulsatile flows. SPI could also be integrated volumetrically (e.g., over the aneurysm sac) as a single objective marker of unstable flow phenotype. Rank-ordering turbulent-like flows based on SPI is indeed possible. That being said, we have only demonstrated this in a single aneurysm case. Furthermore, one limitation is that while SPI is a good descriptor of the most 'active' regions of the WSS, using our exact definition one cannot distinguish between various frequencies. Namely, it cannot discriminate low broadband fluctuations from a high narrowband 'spike', nor does it provide information about which frequencies are dominant. One could, however, decompose SPI into frequency bands, which could be used to highlight instabilities at different frequency ranges. By definition, if those bands are contiguous, those individual SPI would add up to the total SPI. Finally, the cut-off frequency described in the methods was adopted because it can be applied objectively to any driving flow waveform, although future biological investigations may uncover specific frequency bands of interest, and in a broader sample of vascular applications.

5. Conclusion

We have described general frequency-based operators that are easily extendable to other cardiovascular territories, allow for easy separation, isolation, quantification and visualization of low Reynolds number cycle-invariant transient flow instabilities, based on any signal applicable to all spatial dimensions.

6. Conflict of interest statement

The authors have no conflicts of interest to declare.

7. Acknowledgment

Computations were performed on the GPC supercomputer at the SciNet (Loken et al., 2010) HPC Consortium. SciNet is funded by: the Canada Foundation for Innovation under the auspices of Compute Canada; the Government of Ontario; Ontario Research Fund - Research Excellence; and the University of Toronto. The study was supported by The Research Council of Norway through a Centres of Excellence grant to the Center for Biomedical Computing at Simula Research Laboratory, project number 179578. DAS also acknowledges salary support of a Heart & Stroke Foundation Mid-Career Investigator award. CC, DG, FM, UM and DAS acknowledge the partial support of the Joint Project of the Internationalization of research 2014 from Compagnia di San Paolo and Politecnico di Torino.

8. References

Aneurisk-Team, 2012. AneuriskWeb project website, http://ecm2.mathcs.emory.edu/aneuriskweb. Web Site.

Antiga, L., Piccinelli, M., Botti, L., Ene-Iordache, B., Remuzzi, A., Steinman, D. A., 2008. An image-based modeling framework for patient-specific computational hemodynamics. Medical & biological engineering & computing 46 (11), 1097–1112.

Bozzetto, M., Ene-Iordache, B., Remuzzi, A., 2015. Transitional flow in the venous side of patient-specific arteriovenous fistulae for hemodialysis. Annals of biomedical engineering, 1–14.

Chnafa, C., Mendez, S., Nicoud, F., 2014. Image-based large-eddy simulation in a realistic left heart. Computers & Fluids 94, 173–187.

Davies, P. F., Remuzzi, A., Gordon, E. J., Dewey, C. F., Gimbrone, M. A., 1986. Turbulent fluid shear stress induces vascular endothelial cell turnover in vitro. Proceedings of the National Academy of Sciences 83 (7), 2114–2117.

Ferguson, G. G., Nov. 1970. Turbulence in human intracranial saccular aneurysms. Journal of Neurosurgery 33 (5), 485–97.

Fry, D. L., 1968. Acute vascular endothelial changes associated with increased blood velocity gradients. Circulation 22 (2), 165–197.

Gallo, D., Steinman, D. A., Morbiducci, U., 2016. Insights into the co-localization of magnitude-based versus direction-based indicators of disturbed shear at the carotid bifurcation. Journal of biomechanics.

Gelfand, B. D., Epstein, F. H., Blackman, B. R., 2006. Spatial and spectral heterogeneity of time-varying shear stress profiles in the carotid bifurcation by phase-contrast MRI. Journal of Magnetic Resonance Imaging 24 (6), 1386–1392.

Grinberg, L., Yakhot, A., Karniadakis, G. E., 2009. Analyzing transient turbulence in a stenosed carotid artery by proper orthogonal decomposition. Annals of biomedical engineering 37 (11), 2200–2217.

Khan, M., Valen-Sendstad, K., Steinman, D., 2015. Narrowing the expertise gap for predicting intracranial aneurysm hemodynamics: impact of solver numerics versus mesh and time-step resolution. American Journal of Neuroradiology 36 (7), 1310–1316.

Ku, D. N., Giddens, D. P., Zarins, C. K., Glagov, S., 1985. Pulsatile flow and atherosclerosis in the human carotid bifurcation. positive correlation between plaque location and low oscillating shear stress. Arteriosclerosis, Thrombosis, and Vascular Biology 5 (3), 293–302.

Kurokawa, Y., Abiko, S., Watanabe, K., 1994. Noninvasive detection of intracranial vascular lesions by recording blood flow sounds. Stroke 25 (2), 397–402.

Loken, C., Gruner, D., Groer, L., Peltier, R., Bunn, N., Craig, M., Henriques, T., Dempsey, J., Yu, C.-H., Chen, J., et al., 2010. Scinet: lessons learned from building a power-efficient top-20 system and data centre. In: Journal of Physics: Conference Series. Vol. 256(1). IOP Publishing, p. 012026.

Malek, A. M., Alper, S., Izumo, S., 1999. Hemodynamic Shear Stress and Its Role in Atherosclerosis. JAMA 282 (21), 2035–2042.

Morbiducci, U., Kok, A. M., Kwak, B. R., Stone, P. H., Steinman, D. A., Wentzel, J. J., et al., 2016. Atherosclerosis at arterial bifurcations: evidence for the role of haemodynamics and geometry. Thrombosis and haemostasis 115 (3), 484–492.

Mortensen, M., Valen-Sendstad, K., 2015. Oasis: A high-level/high-performance open source navier–stokes solver. Computer Physics Communications 188, 177–188.

Nerem, R., Seed, W., Wood, N., 1972. An experimental study of the velocity distribution and transition to turbulence in the aorta. Journal of Fluid Mechanics 52 (01), 137–160.

Peiffer, V., Sherwin, S. J., Weinberg, P. D., 2013. Computation in the rabbit aorta of a new metric–the transverse wall shear stress–to quantify the multidirectional character of disturbed blood flow. Journal of Biomechanics 46 (15), 2651–2658.

Poelma, C., Watton, P. N., Ventikos, Y., 2015. Transitional flow in aneurysms and the computation of haemodynamic parameters. Journal of The Royal Society Interface 12 (105), 20141394.

Pope, S. B., 2000. Turbulent Flows. Cambridge University Press.

Roach, M. R., Scott, S., Ferguson, G. G., 1972. The hemodynamic importance of the geometry of bifurcations in the circle of Willis (glass model studies). Stroke 3 (3), 255–67.

Simo, J., Armero, F., 1994. Unconditional stability and long-term behavior of transient algorithms for the incompressible navier-stokes and euler equations. Computer Methods in Applied Mechanics and Engineering 111 (1), 111–154.

Taylor, C. A., Steinman, D. A., 2010. Image-based modeling of blood flow and vessel wall dynamics: applications, methods and future directions. Annals of biomedical engineering 38 (3), 1188–1203.

Valen-Sendstad, K., Mardal, K.-A., Mortensen, M., Reif, B. A. P., Langtangen, H. P., 2011. Direct Numerical Simulation of Transitional Flow in a Patient–Specific Intracranial Aneurysm. Journal of Biomechanics 44 (16), 2826–2832.

Valen-Sendstad, K., Mardal, K.-A., Steinman, D. A., 2013. High-resolution CFD detects high-frequency velocity fluctuations in bifurcation, but not sidewall, aneurysms. Journal of Biomechanics 46 (2), 402–407.

Valen-Sendstad, K., Piccinelli, M., KrishnankuttyRema, R., Steinman, D. A., 2015. Estimation of inlet flow rates for image-based aneurysm cfd models: Where and how to begin? Annals of biomedical engineering 43 (6), 1422–1431.

Valen-Sendstad, K., Piccinelli, M., Steinman, D. A., 2014. High-resolution computational fluid dynamics detects flow instabilities in the carotid siphon: Implications for aneurysm initiation and rupture? Journal of biomechanics 47 (12), 3210–3216.

Valen-Sendstad, K., Steinman, D. A., 2014. Mind the gap: Impact of CFD solution strategy on prediction of intra-cranial aneurysm hemodynamics and rupture status. AJNR. American Journal of Neuroradiology 35 (3), 536–543, commentary, 544-545.

Varble, N., Xiang, J., Lin, N., Levy, E., Meng, H., 2016. Flow instability detected by high-resolution computational fluid dynamics in fifty-six middle cerebral artery aneurysms. Journal of biomechanical engineering 138 (6), 061009.

Yagi, T., Sato, A., Shinke, M., Takahashi, S., Tobe, Y., Takao, H., Murayama, Y., Umezu, M., 2013. Experimental insights into flow impingement in cerebral aneurysm by stereoscopic particle image velocimetry: transition from a laminar regime. Journal of The Royal Society Interface 10 (82).

Zajac, J., Eriksson, J., Dyverfeldt, P., Bolger, A. F., Ebbers, T., Carlhäll, C.-J., 2015. Turbulent kinetic energy in normal and myopathic left ventricles. Journal of Magnetic Resonance Imaging 41 (4), 1021–1029.